

1 **Complexation of cationic-neutral block polyelectrolyte with insulin**
2 **and *in vitro* release studies**

3 Natassa Pippa ^{a,b}, Maria Karayianni^b, Stergios Pispas^{b,*}, Costas Demetzos^a

4 ^aDepartment of Pharmaceutical Technology, Faculty of Pharmacy, Panepistimioupolis
5 Zografou 15771, National and Kapodistrian University of Athens, Athens, Greece

6 ^bTheoretical and Physical Chemistry Institute, National Hellenic Research
7 Foundation, 48 Vassileos Constantinou Avenue, 11635, Athens, Greece

8

9 * Corresponding author: Dr. Stergios Pispas, Tel.:+30210-7273824; Fax: +30 210-
10 7273794; E-mail address: pispas@eie.gr

11

12

13 **Abstract**

14

15 Insulin (INS) was incorporated into complexes with the block polyelectrolyte
16 quaternized poly[3,5-bis(dimethylaminomethylene)hydroxystyrene]-b-poly(ethylene
17 oxide) (QNPHOSEO), which is a cationic-neutral block polyelectrolyte. Light
18 scattering techniques are used in order to examine the size, the size distribution and
19 the ζ -potential of the nanocarriers in aqueous and biological media, which are found
20 to depend on the ratio of the components and the physicochemical parameters during
21 and after complex preparation. Circular dichroism and infrared spectroscopy,
22 employed to investigate the structure of the complexed INS, show no alteration of
23 protein structure after complexation. *In vitro* release profiles of the entrapped protein
24 are found to depend on the ratio of the components and the solution conditions used
25 during preparation of the complexes.

26

27 **Keywords:** block polyelectrolyte; insulin; complexation process; stealthiness; *in vitro*
28 release studies

29

30 **1. Introduction**

31 The discovery of insulin revolutionized the use of peptides and proteins as therapeutic
32 agents for several diseases. The evolution of the biotechnological era gave rise to
33 modified insulins to solve some of the bottlenecks in insulin therapy (Pillai, and
34 Panchagnula, 2001; Tibaldi, 2012). Several innovative approaches based on
35 pharmaceutical nanotechnology mimic the endogenous release and kinetics of insulin,
36 and also many improved analogues designed achieve better control and effective
37 treatment of diabetes (Mao et al., 2006; Avadi et al., 2011; Han et al., 2012; Yan et
38 al., 2012).

39
40 Asymmetric amphiphilic block copolymers self-assemble in aqueous media, to form
41 core-shell micellar structures and morphologies, with a mesoscopic or nanoscopic
42 narrow size range and are used for biomedical and pharmaceutical applications (in the
43 order of 10-100 nanometers). Polyelectrolyte block copolymers constitute an
44 intriguing class of bio-inspired macromolecules, as they combine the structural
45 properties of amphiphilic block copolymers, polyelectrolytes and surfactants and
46 provide various possibilities for use as delivery nanosystems of genes and proteins
47 through electrostatic complexation (Al-Tahami and Singh, 2007; Hartig et al., 2007;
48 Pispas, 2007; Reis et al., 2008; Karayianni et al., 2011; Karayianni and Pispas, 2012;
49 Becker et al., 2012; Haladjova et al., 2012; Varkouhi et al., 2012). Polymeric delivery
50 systems based on nanoparticles have emerged as a promising approach for insulin
51 delivery. According to the recent literature, the application of polyion complex
52 micelles into therapeutic fields is rapidly increasing due to simple and efficient
53 encapsulation of biopharmaceuticals (peptides and proteins) and outstanding
54 biocompatibility among various polymer-based drug delivery nanocarriers (Lee and
55 Kataoka, 2009).

56 In the present work we employ dynamic (DLS), static (SLS) and electrophoretic
57 (ELS) light scattering in order to examine the complexation process, as well as the
58 structure and solution behavior in aqueous and biological media of the nanosized
59 complexes, formed between quaternized poly[3,5-
60 bis(dimethylaminomethylene)hydroxystyrene]-b-poly(ethylene oxide) (QNPHOSEO),
61 a cationic-neutral block copolymer, and insulin (INS). Furthermore, the secondary
62 structure of the complexed INS was investigated by means of circular dichroism (CD)
63 and infrared (IR) spectroscopy. Finally, the *in vitro* release of INS from the
64 complexes was studied in physiological conditions. The central goal is to create novel
65 and functional hybrid synthetic/biological macromolecular nanostructures and enrich
66 the basic understanding on behavior motifs in aqueous and biological media, as well
67 as widen application potential of nanostructured polymeric delivery systems with
68 controlled release profile of the encapsulated protein.

69 **2. Materials and Methods**

70

71 **2.1 Materials**

72

73 The synthesis, the physicochemical characterization, as well as the properties of
74 QNPHOSEO are presented extensively in the recent literature (Mountrichas et al.,
75 2006,2007; Mantzaridis et al., 2009; Stepanek et al., 2011). The QNPHOSEO
76 polyelectrolyte block copolymer was characterized by SEC, ¹H-NMR and FTIR and it
77 was found to have the following molecular characteristics: $M_w=98,600$, $M_w/M_n=1.09$,
78 15%wt PEO. The molecular structure of QNPHOSEO is presented in Fig. 1(a).
79 QNPHOSEO chains tend to form loose aggregates in aqueous solutions (Fig. S2)
80 (Stepanek et al., 2011). The QNPHOSEO block polyelectrolyte has been used for
81 DNA and RNA complexation and it was found to have cytotoxicity better than other
82 reference cationic polymers utilized in gene delivery (Varkouli et al., 2012). INS with

83 a molecular weight of 5800 g/mol was purchased from Sigma Aldrich and used
84 without any further purification.

85 *2.1.1 Preparation of QNPHOSEO:INS complexes in different aqueous media*

86 A pH 7 buffer solution was prepared from NaOH and 5mM sodium phosphate.
87 Moreover, 10mM NaCl were added to solution to maintain a fixed ionic strength,
88 along with NaN_3 in a final concentration of 200ppm, in order to avoid bacterial
89 growth. Stock solutions of INS and QNPHOSEO were prepared by dissolving a
90 weighed amount of the dialyzed sample in the appropriate volume of the buffer and
91 the solutions were left to stand overnight for better equilibration.

92 The complexes were prepared by adding different amounts of the INS solutions to
93 QNPHOSEO solutions of the same volume and concentration, under stirring. Finally,
94 appropriate volumes of buffer solutions were added to achieve a constant final volume
95 and ionic strength (equal to that of the buffer solutions) for all solutions prepared.
96 Thus, the concentration of QNPHOSEO was kept constant throughout the series of
97 solutions, while that of INS varied in order to control the required ratio of the two
98 components (or equivalently the [-]/[+] charge ratio of the mixture). The solutions of
99 the complexes developed a bluish tint or turbidity upon mixing, indicating the
100 formation of supramolecular complexes. Subsequently, the solutions of the complexes
101 were left for equilibration overnight, which in some cases resulted in coacervation, i.e.
102 liquid-liquid phase separation of the solution, depending on the INS concentration and
103 pH. Stable solutions were further characterized as discussed below.

104 For the ionic strength dependent light scattering measurements, the ionic strength of
105 the solution was gradually increased by the addition of appropriate aliquots of 1N
106 NaCl solution at pH=7.00 or 7.40, to 1ml of the previously prepared solutions of the
107 complexes. After each addition the solution was rigorously stirred and left to

108 equilibrate for 15min before measurement. Changes in solute concentrations due to
109 NaCl solution addition were taken into consideration in the analysis of the light
110 scattering data.

111

112 2.2.2. *Insulin association efficiency and in vitro INS release studies*

113 The loading and the release of insulin from complexes was investigated by dialysis
114 method. The percentage of INS incorporated into complexes was estimated by
115 spectrophotometry. INS concentration was estimated with the aid of the following
116 INS calibration curve in PBS (pH=7.4):

$$117 \quad \text{INS concentration (mg/ml)} = \frac{\text{absorbance} - 0.0213}{0.2822} \quad (R^2 = 0.9966) \quad (1)$$

118 The absorbance was measured at 277nm. Encapsulation efficiency (EE) was
119 calculated by using the following equation:

$$120 \quad \%EE = \frac{\text{total amount of INS} - \text{free INS}}{\text{total amount of INS (initial)}} \times 100 \quad (2)$$

121 All samples were measured in triplicate and are reported as the mean value.

122 The release profile of INS from the nanovectors was studied in PBS. Nanovectors
123 incorporating INS (1ml of each sample) were placed in dialysis sacks (molecular
124 weight cut off 12,000; Sigma-Aldrich). Dialysis sacks were inserted in 10 mL PBS in
125 shaking water bath set at 37 °C. Aliquots of samples were taken from the external
126 solution at specific time intervals and that volume was replaced with fresh release
127 medium in order to maintain sink conditions. The amount of INS released at various
128 times, up to 10 h, was determined using spectrophotometry at $\lambda_{\text{max}} = 277$ nm with the
129 aid of the calibration curve of the equation (1). All the experiments were carried out in
130 triplicate, and the data presented are the average of the three measurements.

131 **2.2. Methods**

132 *2.2.1. Dynamic and static light scattering*

133 The hydrodynamic radius (R_h) of nanocarriers and the polydispersity Index (PD.I.)
134 were measured by dynamic light scattering (DLS) and the ratio of radius of gyration
135 to hydrodynamic radius (R_g/R_h) was determined by static light scattering (SLS). Mean
136 values and standard deviations were calculated from three independent samples. For
137 dynamic and static light scattering measurements, an AVL/CGS-3 Compact
138 Goniometer System (ALV GmbH, Germany) was used, equipped with a cylindrical
139 JDS Uniphase 22mV He-Ne laser, operating at 632.8 nm, and an Avalanche
140 photodiode detector. The system was interfaced with an ALV/LSE-5003 electronics
141 unit, for stepper motor drive and limit switch control, and an ALV-5000/EPP multi-
142 tau digital correlator. Autocorrelation functions were analyzed by the cumulants
143 method and the CONTIN software. Apparent hydrodynamic radii, R_h , at finite
144 concentrations, were calculated by aid of the Stokes - Einstein equation:

$$145 \quad R_h = \frac{k_B T}{6\pi\eta_0 D} \quad (3)$$

146 where k_B is the Boltzmann constant, η_0 is the viscosity of water at temperature T, and
147 D is the diffusion coefficient at a fixed concentration. The polydispersity of the
148 particle sizes was given as the μ_2/Γ^2 (PD.I.) from the cumulants method, where Γ is
149 the average relaxation rate, and μ_2 is its second moment.

150 Light scattering has been used widely in the study of the fractal dimensions of
151 aggregates. In static light scattering, a beam of light is directed into a sample and the
152 scattered intensity is measured as a function of the magnitude of the scattering vector
153 q, with:

154
$$q = \frac{4\pi n_0}{\lambda_0} \sin\left(\frac{\theta}{2}\right) \quad (4)$$

155 where n_0 is the refractive Index of the dispersion medium, θ is the scattering angle and
156 λ_0 is the wavelength of the incident light. Measurements were made at the angular
157 range of 30° to 150° (i.e. the range of the wave vector was $0.0067 < q < 0.025 \text{ nm}^{-1}$).

158 The general relation for the angular dependence of the scattered intensity, $I(q)$ is:

159
$$I(q) \sim q^{-d_f} \quad (5)$$

160 where d_f is the fractal dimension of the aggregates with $1 \leq d_f \leq 3$ ($d_f=3$ corresponds to
161 the limit of a completely compact Euclidean sphere where less compact structures are
162 characterized by lower d_f values). The above equation is the classical result used to
163 determine the mass fractal dimension from the negative slope of the linear region of a
164 log-log plot of I vs. q .

165 2.2.2. Electrophoretic mobility – microelectrophoresis

166 The zeta potential (ζ -potential) plays an important role in colloidal stability of
167 nanoparticles and can be readily measured by the technique of microelectrophoresis.

168 The zeta potential of chimeric nanostructures was measured using Zetasizer
169 3000HAS, Malvern Instruments, Malvern, UK. 50 μ l of the dispersions was 30-fold
170 diluted in dispersion medium and ζ -potential was measured at room temperature at
171 633nm. The zeta potentials were calculated from electrophoretic mobilities, μ_E , by
172 using the Henry correction of the Smoluchowski equation:

173
$$\zeta = \frac{3\mu_E n}{2\varepsilon_0 \varepsilon_r} \frac{1}{f(\kappa a)} \quad (6)$$

174 where ϵ_0 is the permittivity of the vacuum, ϵ_r is the relative permittivity, α is the
175 particle radius, κ is the Debye length, and η is the viscosity of water. The function
176 $f(\kappa\alpha)$ depends on particle shape. While if $\kappa\alpha > 1$:

$$177 \quad f(\kappa\alpha) = 1.5 + \frac{9}{2(\kappa\alpha)} + \frac{75}{2(\kappa\alpha)^2} \quad (7)$$

178 The above function refers to dispersions of the present study.

179 *2.2.3. Circular dichroism*

180 CD measurements were conducted using a JASCO-715 (Jasco Corp., Tokyo, Japan)
181 spectropolarimeter with a Peltier-type cell holder, which allows for temperature
182 control. Wavelength scans in the far UV region (190 to 260 nm) were performed in
183 Quartz SUPRASIL (HELLMA, GmbH & Co., Müllheim, Germany) precision cells of
184 0.1 cm path length. Each spectrum was obtained by averaging three successive
185 accumulations with a wavelength step of 0.5 nm at a 100 nm/min rate, response time
186 4 s, and bandwidth 5 nm. The absorption spectra were recorded selecting the UV
187 (single) mode of the instrument. An estimation of the secondary structure elements
188 was obtained by analyzing the CD spectra using the CDNN algorithm.

189 *2.2.4. Infrared spectroscopy*

190 Infrared spectra of the protein, polyelectrolyte block copolymer and complexes in thin
191 film form were acquired at room temperature in the range 5000-550 cm^{-1} , using a
192 Fourier transform instrument (Bruker Equinox 55), equipped with a single bounce
193 attenuated total reflectance (ATR) diamond accessory from SENS-IR. A small aliquot
194 of each solution was placed on the ATR element and dried under N_2 flow before
195 measurement. For each sample the final spectrum is the average of the three 100-scan

196 measurements at 2cm^{-1} resolution. The measurement of each sample was bracketed by
197 two background spectra in order to allow the elimination of H_2O vapor bands by
198 interpolation.

199 **3. Results and Discussion**

200 *3.1. Physicochemical characterization of QNPHOSEO:INS complexes in aqueous and* 201 *biological media*

202 The complexation process between the QNPHOSEO polyelectrolyte and INS at $\text{pH}=7$
203 and $I=0.01\text{M}$, and in PBS ($\text{pH}=7.40$ and $I=0.154\text{M}$) was first investigated by means of
204 dynamic light scattering. It should be noted that PBS ($\text{pH}=7.40$) was chosen as
205 dispersion medium because the pH and the ionic strength of PBS resembles the
206 conditions met within the human body. At $\text{pH}=7$ the electrostatic interactions of the
207 system are expected to be strong, since the QNPHOSEO polyelectrolyte block carries
208 two positively charged groups per functionalized monomeric unit and INS has a net
209 negative charge of -4 . The obtained results from DLS measurements at 90° regarding
210 the values of the hydrodynamic radius, R_h , and the light scattering intensity, I_{90} ,
211 (corrected for the concentration increase) are shown in Figs. 2(a) and (b), as function
212 of the protein concentration, C_{INS} , in the solutions of the complexes. The structure and
213 the formation process of QNPHOSEO:INS complexes is represented in Fig. 1(a).

214 The concentration of QNPHOSEO copolymer is kept constant throughout the series
215 of aqueous solutions of different ionic strength investigated. It should be pointed out
216 that at high INS concentration; coacervation of the solutions of the complexes took
217 place, only at $\text{pH}=7$ and $I=0.01\text{M}$ NaCl. This phenomenology was not observed for
218 the solutions in PBS. DLS results at low ionic strength ($I=0.01\text{M}$) show that all
219 solutions exhibit a main peak at high R_h values ($\sim 80\text{nm}$), which apparently
220 corresponds to the formed mixed aggregates (QNPHOSEO:INS complexes) and a

221 significantly smaller one at lower R_h values, which most probably denotes the
222 presence of a small number of free unimer diblock copolymer chains in solution. The
223 values of the scattering intensity, I_{90} , which is proportional to the mass of the species
224 in solution, increased gradually as a function of C_{INS} , providing proof of the occurring
225 complexation (Fig.2(b)), i.e. the mass of the complexes increases as C_{INS} increases.
226 As protein concentration increases each polyelectrolyte chain interacts with an
227 increasing number of protein molecules, the degree of charge neutralization becomes
228 higher and the size distribution of the complexes decreases, especially at the highest
229 ionic strength (Becker et al., 2012). In contrast I_{90} (or the mass of the complexes)
230 shows a more steep increase in the case of PBS solutions, although the protein
231 concentration range studied in these systems is wider due to the absence of
232 coacervation. In pH=7, we observed aggregation of the complexes and precipitation
233 of the supramolecular aggregates, when the initial concentration of insulin was higher
234 than 0.07mg/ml. ζ -potential decreases in absolute value as the concentration of the
235 protein increases in PBS, or equivalently the effective positive charge of the
236 complexes reduces as a function of the protein concentration (Fig. 3(a)). On the other
237 hand, ζ -potential values remained unaffected in the lowest ionic strength solutions. It
238 seems that the ionic strength of the solution plays a significant role in the interactions
239 and the structure of the resulting complexes. Due to the primary aggregation of
240 QNPHOSEO chains in aqueous media we expect interactions between QNPHOSEO
241 aggregates with INS molecules and this initial state of the block polyelectrolyte may
242 have a significant effect on the structure of resulting QNPHOAE0:INS complexes
243 under different solution conditions. We also investigated the morphology of the
244 complexes via their fractal dimension (d_f), determined by static light scattering.
245 Although the nanosystems developed in this study are polydisperse in size we can still

246 make use of this parameter to extract information on morphological changes, since
247 size polydispersity is expected to influence the d_f results of the nanosystems in more
248 or less a similar way (after all the PDI index values determined by cumulant analysis
249 lie in the range 0.2-0.3). d_f was found near to 1.6 for QNPHOSEO:INS aggregates in
250 PBS (Fig. S4). An increase of d_f values was observed for QNPHOSEO:INS
251 complexes in buffer at pH=7.00 as the concentration of the protein increases (Fig.
252 S4), although the concentration range studied in these systems is narrow due to
253 coacervation. This observation may be associated by a small change in the
254 density/morphology of the complexes as INS concentration increases in this case.

255 The values of R_g/R_h were also calculated (Fig 3.(b)) from multiangle light scattering
256 measurements. This ratio is sensitive to the shape of particles in solution and can be
257 used as a rough estimate of the internal morphology of the particles formed after
258 complexation. This is based on the notion that R_g is a measure of the mass density
259 distribution around the center of the structure, while R_h defines the outer dimensions
260 of the particle. According to Burchard (1983), the R_g/R_h ratio takes the values of 0.775
261 for a hard uniform sphere and 1.0 for vesicles with thin walls, while values of 1.3 to
262 1.5 indicate a random coil (loose) conformation in the case of macromolecular chains.
263 In the present case, the R_g/R_h values are near 1.00 for QNPHOSEO:INS in PBS at low
264 INS concentration. These results may indicate a more well-defined hollow sphere
265 (vesicle like) structure for the complexes (Fig 3.(b)) or a rather low density full
266 spherical structure. It should be pointed out that the morphology of mixed aggregates
267 changes significantly as the concentration of the INS increases (as indicated from
268 R_g/R_h values) (Fig. 3(b)). At highest concentration of INS ($C_{INS} > 1 \times 10^{-4}$ g/mL), open
269 (low density) spherical structures are observed for QNPHOSEO:INS complexes (Fig.
270 2(e)). On the other hand, the R_g/R_h values indicate open (low density) spherical

271 structures for aggregates in the pH=7 buffer of low ionic strength (Fig 3.(b)). These
272 differences may be a result of the differences in the salinity of the media, especially at
273 the lower concentration of INS.

274 According to the literature, it is important to characterize the physicochemical
275 properties of the complexes formed under different conditions in biological media,
276 like fetal bovine serum (FBS), because interaction with the proteins of the medium is
277 expected to alter the physicochemical properties of the nanostructures, thereby
278 affecting their stability and clearance properties (Arnida Jánat-Ambury et al., 2011).
279 We investigated the physicochemical characteristics of QNPHOSEO:INS complexes
280 in Fetal Bovine Serum (FBS). The prepared complexes in aqueous media were diluted
281 in FBS:PBS 10% v/v (Arnida Jánat-Ambury et al., 2011; Pippa et al., 2012a,b,
282 2013a,b).. The size of the complexes in biological medium (FBS) was increased from
283 ca. 50 nm to ca. 200 nm, as a function of INS concentration, compared to the initial
284 solutions after complex formation (Figs. 4(a) and 5(a)). In all cases, the
285 supramolecular aggregates of insulin carrier complexes and plasma proteins remained
286 smaller than 300nm (within the nanoparticle scale which is important for
287 nanomedicinal purposes). The values of the scattering intensity, I_{90} , which is
288 proportional to the mass of the species in solution, did increase in FBS, providing
289 proof of some additional, but of relatively low extent, complexation of the block
290 copolymer/INS nanoparticles with components of FBS, especially in PBS. This
291 observation indicates that QNPHOSEO copolymer imparts stealth properties and
292 stability in the complexes, due to the presence of PEO chains that shield the
293 complexes (it should be noted that no precipitation of the complexes was observed
294 when in contact with FBS solutions). A shift of ζ -potential of the complexes to
295 negative values is observed, presumably due to some binding of FBS proteins, which

296 can alter the nanoparticle's effective size and surface properties (the main protein
297 component of FBS is albumin which carries a negative charge at physiological
298 conditions) (Fig.4(b) and 5(b) (Arnida Jánat-Ambury et al., 2011; Pippa et al.,
299 2012a,b, 2013a,b). The shift of the ζ -potential to negative values explains the absence
300 of precipitation of the complexes, because of additional electrostatic stabilization of
301 the aggregates. In our opinion, these differences are not statically significant and,
302 although there is some protein adsorption on the complexes, their size and surface
303 properties still remain within the limits allowing the use of the present nanosystems as
304 nanocarriers of insulin.

305 *3.2. Effect of ionic strength*

306 The increase of the ionic strength in the solutions of the complexes induces charge
307 screening and weakening of the electrostatic interactions, so it is expected to greatly
308 influence the solution behavior and structure/morphology of the preformed
309 complexes. In order to investigate this effect, DLS/SLS measurements as a function of
310 the added NaCl concentration were conducted, and the resulting R_h and I_{90} (corrected
311 for the difference in concentration) values for representative solutions of
312 QNPHOSEO:INS complexes formed at low and high C_{INS} values at pH 7 and 7.40 are
313 shown in Figs. S5 and 6. In the case of complexes prepared at low ionic strength
314 buffer R_h does not change significantly with an increase of the ionic strength (Fig.
315 S5(a)). There is a rather small gradual increase of their size. We recall that at low C_{INS}
316 values the number of interacting protein molecules per polyelectrolyte chain is rather
317 small, while at high C_{INS} values the formed complexes are characterized by rather
318 large number of interacting protein molecules per polyelectrolyte chain (Fig. 5(a))
319 (Karayianni et al., 2011). Light scattering intensity behavior is different for complexes
320 formed at low and at high INS concentration. At low INS concentration I_{90} (and mass

321 of the complexes) increases, and then drops with ionic strength increase meaning that
322 there is some additional aggregation of the complexes at low ionic strengths (but
323 higher than the initially used ones for complex formation) and by increasing salt
324 concentration the mass decreases again (Fig. 6(b)). In the case of complexes formed at
325 higher INS concentration there are very small intensity changes (and mass changes)
326 with added salt (Fig. S5(b)), which shows rather a small decrease in the mass of the
327 complexes. R_g/R_h values for these systems show a decrease and a plateau at $I > 0.1$ M,
328 reaching at an R_g/R_h value ca. 0.9-1.0, which in turn may indicate more compact
329 spherical structures than the initial ones. The observed behavior should be attributed
330 to charge screening effects that weaken electrostatic interactions and promote
331 hydrophobic effects. Due to the hydrophobic nature of the QNPHOSEO chains and
332 their initial aggregation state, addition of salt may result in secondary aggregation or
333 disruption of the complexes, depending on the initial conditions during complex
334 formation.

335 The hydrodynamic radius of the complexes, as a function of the added NaCl
336 concentration, remained more or less unaffected in the case of complexes formed in
337 PBS buffer (Fig. 6(a)). The same is true for the mass of the complexes as indicated by
338 the I_{90} values (Fig. 6(b)). The morphology of the complexes showed some changes
339 with more compact spherical structures being observed at higher salt concentrations,
340 as indicated from the decrease in R_g/R_h values (Fig. 6(c)) (Karayianni et al., 2011).
341 For these systems changes in the determined parameters are small and rather smooth.
342 This may imply that the QNPHOSEO:INS complexes formed in PBS are more stable
343 to ionic strength increase and may also have a structure closer to equilibrium.

344 *3.3. Protein structure within the complexes*

345 The preservation of the enzymatic activity, which is directly correlated with the
346 protein conformation, is an issue of major importance in most applications involving
347 protein-polyelectrolyte complexes. For this reason, the structure of complexed protein
348 was monitored via circular dichroism and infrared spectroscopic techniques, and
349 representative results of QNPHOSEO:INS system at pH=7.40 and 0.154M NaCl are
350 presented below.

351 Firstly, circular dichroism (CD) was employed for the determination of the complexed
352 protein structure. Fig. 7(a) presents the measured far-UV CD spectra of three
353 representative solutions at $C_{INS}=0.07, 0.26$ and 0.4 mg/ml of QNPHOSEO:INS
354 system at pH=7.40 and 0.154M NaCl, and of neat INS at 1 mg/ml concentration and
355 same solution conditions. As it can be seen, only small changes in the CD spectra
356 between the neat and the complexed INS are observed. The analysis of the spectra
357 carried out using the CDNN algorithm yielded similar results and the average
358 percentages of protein secondary structure are summarized in Table S1. Obviously,
359 the percentages of protein secondary structure are preserved for all solutions of the
360 complexes, thus proving that the complexation does not cause structural disruption of
361 the protein (Bouchard et al., 2000).

362 Moreover, infrared (IR) spectroscopy measurements were performed and Fig. 7(b)
363 shows the IR spectra of the same three representative solutions at $C_{INS}=0.07, 0.26$ and
364 0.4 mg/ml of QNPHOSEO:INS system at pH=7.40 and 0.154M NaCl in the Amide I
365 and II region, including the corresponding spectrum of neat INS for comparison. The
366 spectra have been normalized to the intensity of the Amide I band, after subtraction of
367 the spectral contribution of the neat block polyelectrolyte copolymer. The constancy
368 of the Amide I and II profiles, peaking at ca. 1658 and 1540 cm^{-1} respectively,
369 indicates the absence of significant protein configuration changes, such as those

370 observed upon denaturation (Bouchard et al., 2000). Therefore, it can be concluded
371 that insulin preserves its structure and activity after complexation.

372 *3.4. Encapsulation efficiency and in vitro release of INS*

373 Values of encapsulation efficiency varied from 10 to 40% for the different
374 formulation as seen in Table S2. They were particularly affected by the dispersion
375 medium and by the initial concentration of INS. Encapsulation efficiency increased
376 with the increase of the initial concentration of the protein in the two aqueous
377 dispersion media. The *in vitro* release of the INS from the nanocomplexes, at different
378 molar ratios of the protein component, is presented in Fig. 8. It is observed that the *in*
379 *vitro* release of the INS from the prepared polyelectrolyte aggregates is quite fast
380 especially for the QNPHOSEO:INS nanoparticles of initial concentration of INS was
381 0.067 mg/ml (Fig. 8). Full insulin release was only observed with QNPHOSEO:INS
382 nanoparticles (initial concentration of INS was 0.067 mg/ml during complex
383 formation) after 50min (Fig. 8). Up to 80% of the insulin was released almost
384 immediately from QNPHOSEO:INS nanoparticles (initial concentration of INS was
385 0.027 mg/ml). Full insulin release was also observed with QNPHOSEO:INS
386 nanoparticles (initial concentration of INS was 0.260 mg/ml) after 8 hours (Fig. 8).
387 Biphasic drug release patterns were observed for this formulation. The release kinetics
388 of INS from this nanosystem follow zero order kinetics, but separated in two phases
389 with two distinct rates, an initial faster one followed by a slower one (Fig. 8). In our
390 opinion, the determining factor of the release profile of the INS is the initial
391 concentration of the protein, which affects the physicochemical and morphological
392 characteristics of the complexes and consequently the release kinetics. From the
393 application point of view, it can be concluded that encapsulation and release of insulin
394 in the present nanosystems can be controlled via the ratio of the two components and

395 to a lesser extend by the physicochemical parameters of solution during initial
396 complex formation.

397

398 **4. Conclusions**

399 We have studied the electrostatic complexation process between the block
400 polyelectrolyte quaternized poly[3,5-bis(dimethylaminomethylene)hydroxystyrene]-
401 b-poly(ethylene oxide) (QNPHOSEO), which is a cationic-neutral polyelectrolyte,
402 and INS. It was shown that the structure and solution behavior of the formed
403 complexes depend on the ratio of the two components, as well as on the pH and the
404 ionic strength of the solution during complex preparation. This study provides
405 interesting and useful new insights into the interaction mechanism between oppositely
406 charged block polyelectrolyte loose aggregates with stealth properties and proteins.
407 The increase of the ionic strength in the solutions of the complexes induces charge
408 screening and weakening of the electrostatic interactions that lead to different
409 structures of the complexes. The size of complexes in biological medium (FBS) was
410 not increased significantly. This observation indicates that QNPHOSEO copolymer
411 imparts biological stability in the complexes. Moreover, the native protein structure is
412 preserved upon complexation. Encapsulation efficiency increased with the increase of
413 the initial concentration of the protein in PBS. The *in vitro* release of the INS from the
414 prepared polyelectrolyte aggregates is quite slow especially for the QNPHOSEO:INS
415 nanoparticles with the higher initial concentration of INS. The results of our study
416 contribute to the overall scientific efforts to prepare efficient carriers for INS and
417 could be useful in order to develop nanocarriers with increased efficacy, safety and
418 tolerability. The prepared nanocarriers can disclose the pharmacokinetic reality of
419 behavior of INS and improve its therapeutic value and side effects. This is because of
420 the interdependence of particle size distribution and physicochemical characteristics,

421 coupled with the beneficial effects of different biomaterials on biological and
422 pharmacokinetic processes.

423

424 **Acknowledgements**

425

426 Authors acknowledge financial support of the work by the NANOMACRO 1129

427 project which is implemented in the framework of the Operational Program

428 “Education and Life-long Learning” (Action “ARISTEIA I”) and it is co-funded by

429 the European Union (European Social Fund) and by national funds.

430

431 **References**

432

433 Arnida Janát-Amsbury, M.M., Ray, A., Peterson, C.M., Chandehari, H., 2011.
434 Geometry and surface characteristics of gold nanoparticles influence their distribution
435 and uptake by macrophages. *Eur. J. Pharm. Biopharm.* 77,417-423.

436 Al-Tahami, K., Singh, J., 2007. Smart polymer based delivery systems for proteins
437 and proteins. *Recent Pat. Drug Deliv. Formul.*1,65-71.

438

439 Avadi, M.R., Sadeghi, A.M., Mohamadpour Dounighi, N., Dinarvand, R., Atyabi, F.,
440 Rafiee-Tehrani, M., 2011. Ex vivo evaluation of insulin nanoparticles using chitosan
441 and Arabic gum. *ISRN Pharm.* 2011,860109.

442 Becker, A.L., Henzler, K., Welsch, N., Ballauff, M., Borisov, O., 2012. Proteins and
443 polyelectrolytes: A charged relationship. *Curr. Opin. Colloid. Interface Sc.* 17,90-96

444

445 Bouchard, M., Zurdo, J., Nettleton, E.J., Dobson, C.M., Robinson, C.V., 2000.
446 Formation of insulin amyloid fibrils followed by FTIR simultaneously with CD and
447 electron microscopy. *Protein Science* 9,1960-1967.

448

449 Burchard, W., 1983. Static and dynamic light scattering from branched polymers and
450 biopolymers. *Adv. Polym. Sci.* 48,1-124

451

452 Haladjova, E., Rangelov, S., Tsvetanov, C.B., Pispas, S. 2012. DNA encapsulation via
453 nanotemplates from cationic block copolymer micelles. *Soft Matter* 8, 2884-2889

454 Han, L., Zhao, Y., Yin, L., Li, R., Liang, Y., Huang, H., Pan, S., Wu, C., Feng, M.,
455 2012. Insulin-loaded pH-sensitive hyaluronic acid nanoparticles enhance transcellular
456 delivery. *AAPS Pharm. Sci. Tech.* 13,836-845.

457 Hartig, S.M., Greene, R.R., DasGupta, J., Carlesso, G., Dikov, M.M., Prokop, A.,
458 Danidson, J.M. 2007. Multifunctional nanoparticulate polyelectrolyte complexes.
459 *Pharm. Res.* 24,2353-2369.

460 Karayianni, M., Pispas, S., Chryssikos, G.D., Gionis, V., Giatrellis, S., Nounesis, G.,
461 2011. Complexation of lysozyme with poly(sodium (sulfamate-carboxylate)isoprene).
462 *Biomacromolecules* 12,1697-1706

463 Karayianni, M., Pispas, S., 2012. Complexation of stimuli-responsive star-like
464 amphiphilic block polyelectrolyte micelles with lysozyme. *Soft Matter* 8,8758-8769.

465 Lee, Y., Kataoka, K., 2009. Biosignal-sensitive polyion complex micelles for the
466 delivery of biopharmaceuticals. *Soft Matter* 5,3810-3817.

467 Mantzaridis, C., Mountrichas, G., Pispas, S., 2009. Complexes between high charge
468 density cationic polyelectrolytes and anionic single- and double-tail surfactants. *J.*
469 *Phys. Chem. B* 113,7064-7070.

470 Mao, S., Bakowsky, U., Jintapattanakit, A., Kissel, T., 2006. Self-assembled
471 polyelectrolyte nanocomplexes between chitosan derivatives and insulin. *J. Pharm.*
472 *Sci.* 95,1035-1048.

473 Mountrichas, G., Mantzaridis, C., Pispas, S., 2006. Well-defined flexible
474 polyelectrolytes with two cationic sites per monomeric unit. *Macromol. Rapid.*
475 *Comm.* 27,289-294.

476 Mountrichas, G., Pispas, S., 2007. Novel double hydrophilic block copolymers based
477 on poly(p-hydroxystyrene) derivatives and poly(ethylene oxide). *J. Polym. Sci. Part.*
478 *A: Polym. Chem.* 45,5790-5799.

479 Pillai, O., Panchagnula, R., 2001. Insulin therapies –past, present and future. *Drug*
480 *Discov. Today* 6,1056-1061.

481 Pippa, N., Pispas, S., Demetzos, C., 2012a. The fractal hologram and elucidation of
482 the structure of liposomal carriers in aqueous and biological media. *Int. J. Pharm.*
483 430,65-73

484 Pippa, N., Pispas, S., Demetzos, C., 2012b. The delineation of the morphology of
485 charged liposomal vectors via a fractal analysis in aqueous and biological media:
486 physicochemical and self-assembly studies. *Int. J. Pharm.* 437,264-274.

487 Pippa, N., Kaditi, E., Pispas, S., Demetzos, C., 2013a. PEO-b-PCL/DPPC chimeric
488 nanocarriers: self-assembly aspects in aqueous and biological media and drug
489 incorporation. *Soft Matter* 9,4073-4082.

490 Pippa, N., Kaditi, E., Pispas, S., Demetzos, C., 2013b. DPPC/poly(2-methyl-2-
491 oxazoline)-grad-poly(2-phenyl-2-oxazoline) chimeric nanostructures as potential drug
492 nanocarriers. *J. Nanopart. Res.* 15,1685.

493 Pispas, S., 2007. Complexes of lysozyme with sodium (sulfamate-
494 carboxylate)isoprene/ethylene oxide double hydrophilic block copolymers. *J. Polym.*
495 *Sci. Part A: Polym. Chem.* 45,509-520.

496 Reis, C.P., Ribeiro, A.J., Veiga, F., Neufeld, R.J., Damgé, C., 2008. Polyelectrolyte
497 biomaterial interactions provide nanoparticulate carrier for oral insulin delivery. *Drug*
498 *Deliv.* 15,127-139.

499 Stepanek, M., Matejicek, P., Prochazka, K., Filippov, S.K., Angelov, B., Slouf, M.,
500 Mountrichas, G., Pispas, S., 2011. Polyelectrolyte-surfactant complexes formed by
501 poly-[3,5-bis(trimethylammoniummethyl)-4-hydroxystyrene iodide]-block-

502 poly(ethylene oxide) and sodium dodecyl sulfate in aqueous solutions. *Langmuir* 27,
503 5275-5281.

504 Tibaldi, J.M., 2012. Evolution of insulin development: focus on key parameters. *Adv.*
505 *Ther.* 29,590-619.

506 Varkouhi, A.K., Mountrichas, G., Schiffelers, R.M., Lammers, T., Storm, G., Pispas,
507 S., Hennik, W.E., 2012. Polyplexes based on cationic polymers with strong nucleic
508 acid binding properties. *Eur. J. Pharm. Sci.* 45,459-466.

509 Yan, Y., Wei, D., Li, J., Zheng, J., Shi, G., Luo, W., Pan, Y., Wang, J., Zhang, L., He,
510 X., Liu, D., 2012. A poly(L-lysine)-based hydrophilic star block co-polymer as a
511 protein nanocarrier with facile encapsulation and pH-responsive release. *Acta*
512 *Biomater.* 8,2113-2120.

513

514

515

516

517

518

519

520

521

522

523

524

525

526

527

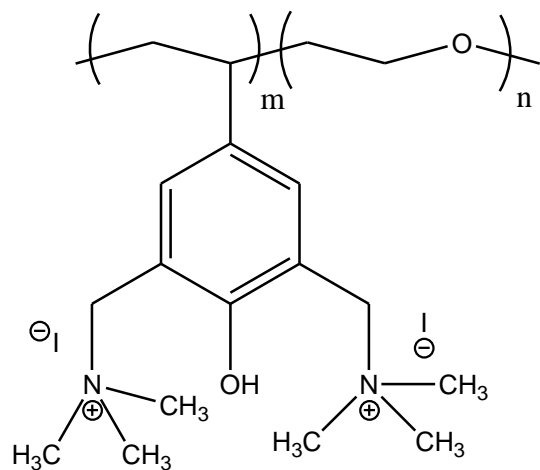
528

529

530

531

532 **Figures**



b.

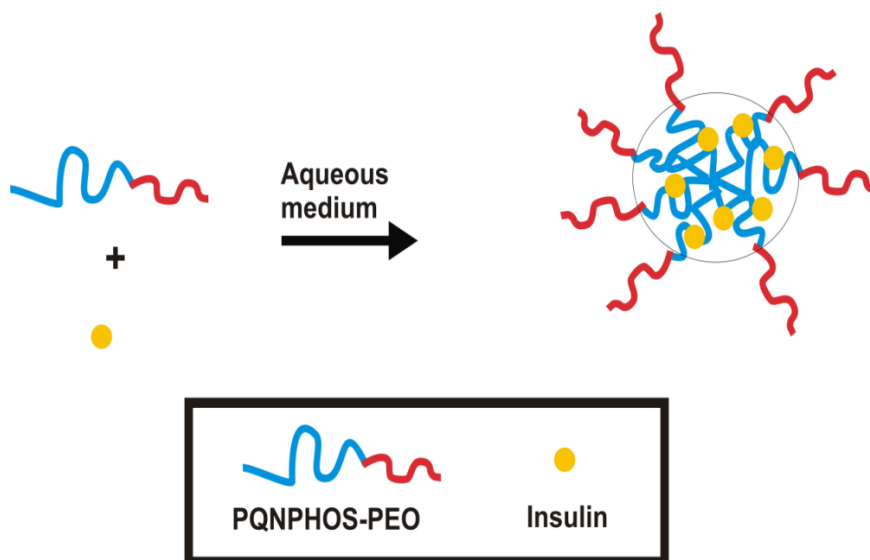
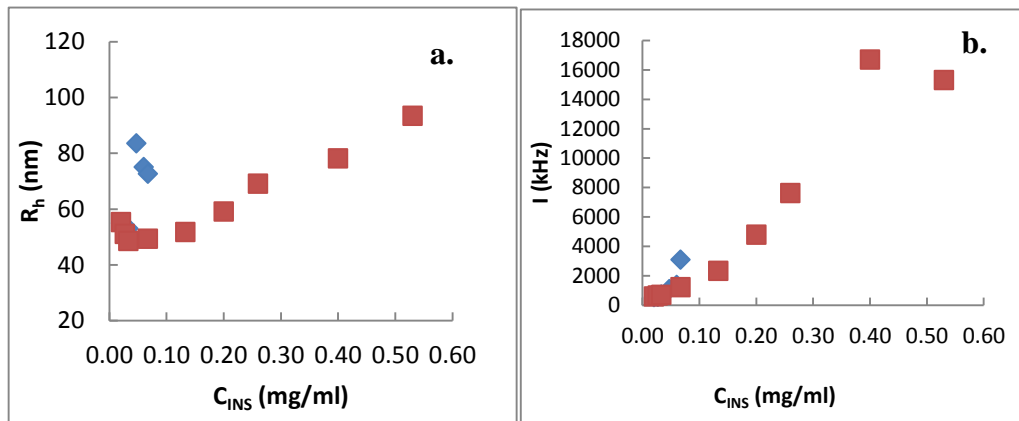


Figure 1. a. Molecular structure of QNPHOSEO block polyelectrolyte (the degrees of polymerization are $m=162$ and $n=334$) **b.** Schematic representation of the formation of QNPHOSEO:INS complexes.

542

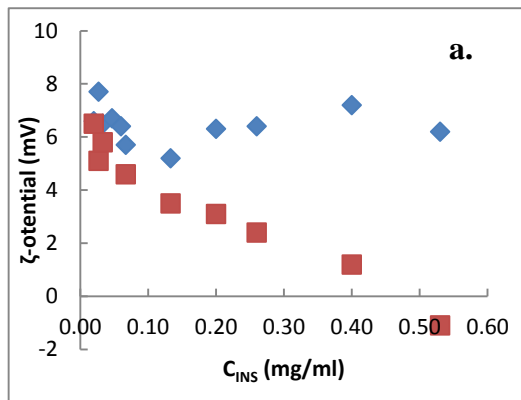


543

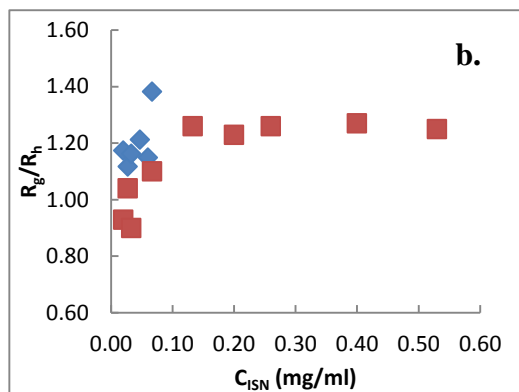
544 **Figure 2.** (a) Hydrodynamic radius, R_h , and (b) light scattering intensity at 90° , I , as
545 a function of C_{INS} , for the solutions of QNPHOSEO:INS system at pH=7.00 and
546 0.01M NaCl (blue points) and at pH=7.40 and 0.154M NaCl (red points).

547

548



549



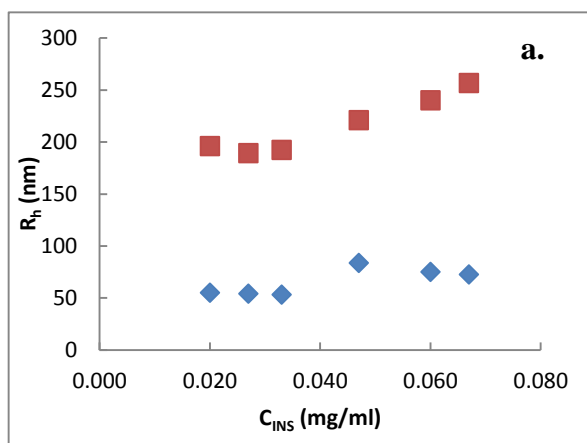
550

551 **Figure 3.** (a) ζ -potential and (b) R_g/R_h as a function of C_{INS} , for the solutions of
552 QNPHOSEO:INS system at pH=7.00 and 0.01M NaCl (blue points) and at pH=7.40
553 and 0.154M NaCl (red points).

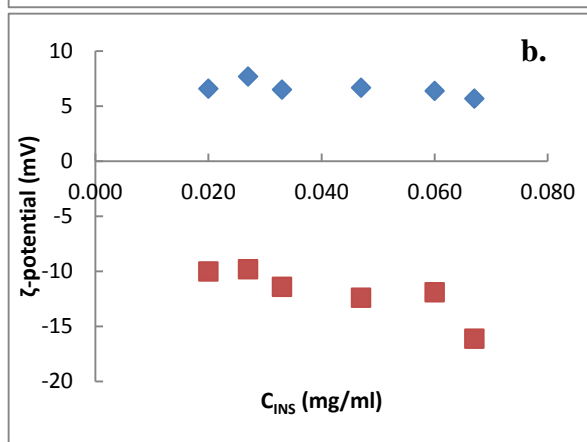
554

555

556



557



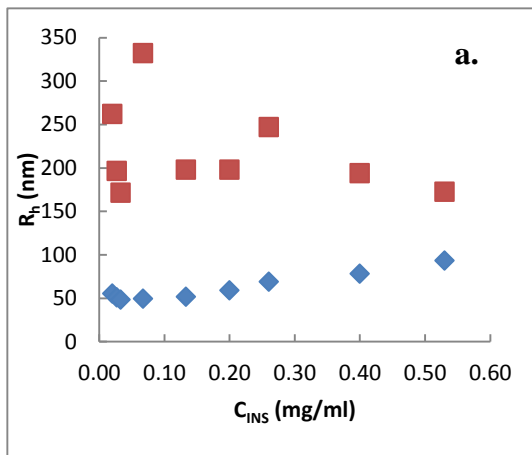
558

559

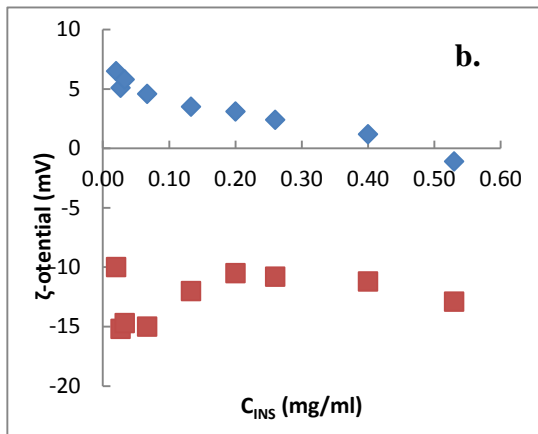
560 **Figure 4. (a)** Hydrodynamic radius, R_h , and **(b)** ζ -potential as a function of C_{INS} , for
 561 the solutions of QNPHOSEO:INS complexes as prepared at pH=7 and 0.01M NaCl
 562 (blue points) and after dilution in FBS:PBS 10% (v/v) (red points).

563

564



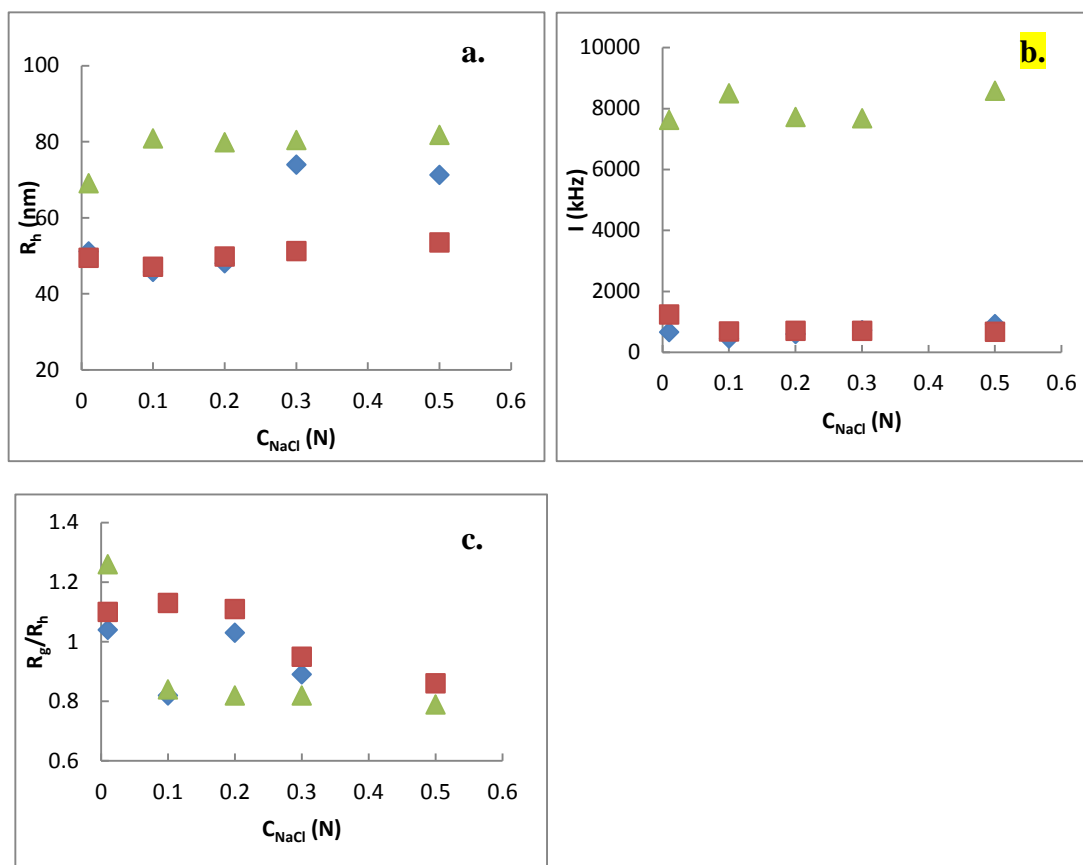
565



566

567 **Figure 5.** (a) Hydrodynamic Radius, R_h , and (b) ζ -potential as a function of C_{INS} , for
 568 the solutions of QNPHOSEO:INS complexes as prepared at pH=7.40 and 0.154M
 569 NaCl (blue points) and after dilution in FBS:PBS 10%(v/v) (red points).

570



571

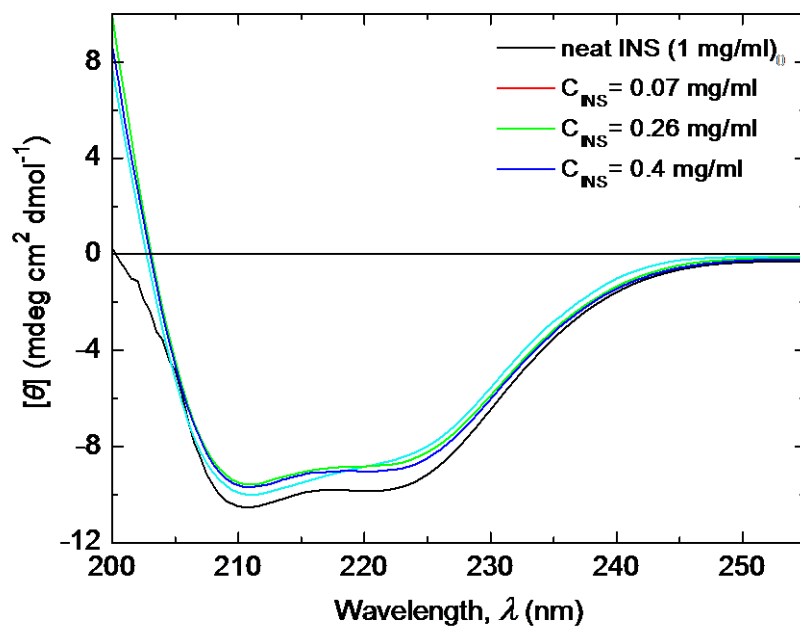
572

573 **Figure 6.** (a) Hydrodynamic radius, R_h , (b) light scattering intensity at 90°, I , and (c)
 574 R_g/R_h , as a function of the added NaCl concentration of representative solutions,
 575 corresponding to low ($C_{INS}=0.027\text{mg/ml}$ –blue points and $C_{INS}=0.067\text{mg/ml}$ –red
 576 points) and high ($C_{INS}=0.260\text{mg/ml}$ –green points) C_{INS} , of the QNPHOSEO:INS
 577 complexes prepared at $\text{pH}=7.4$ and $I=0.154\text{M}$.

578

579

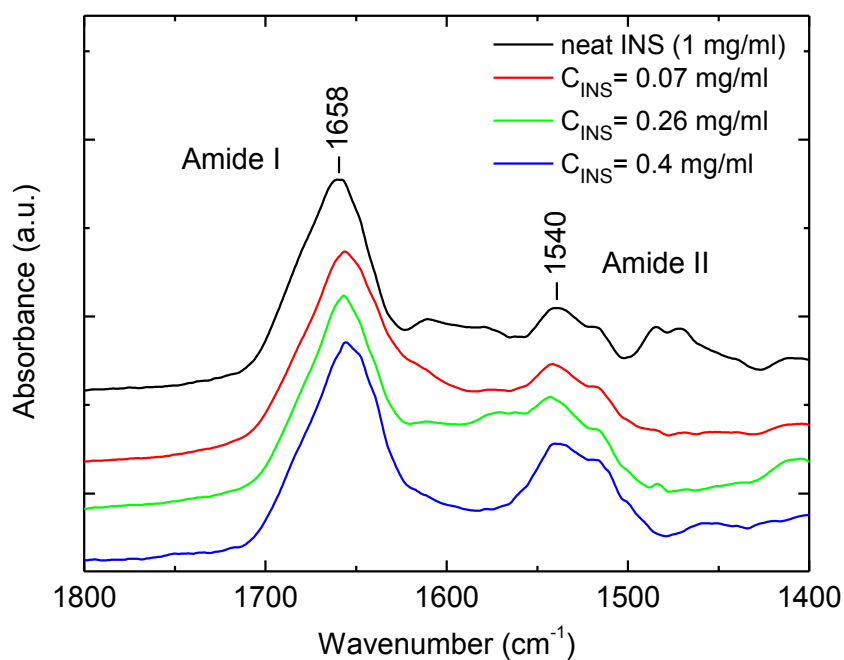
a.



580

b.

581

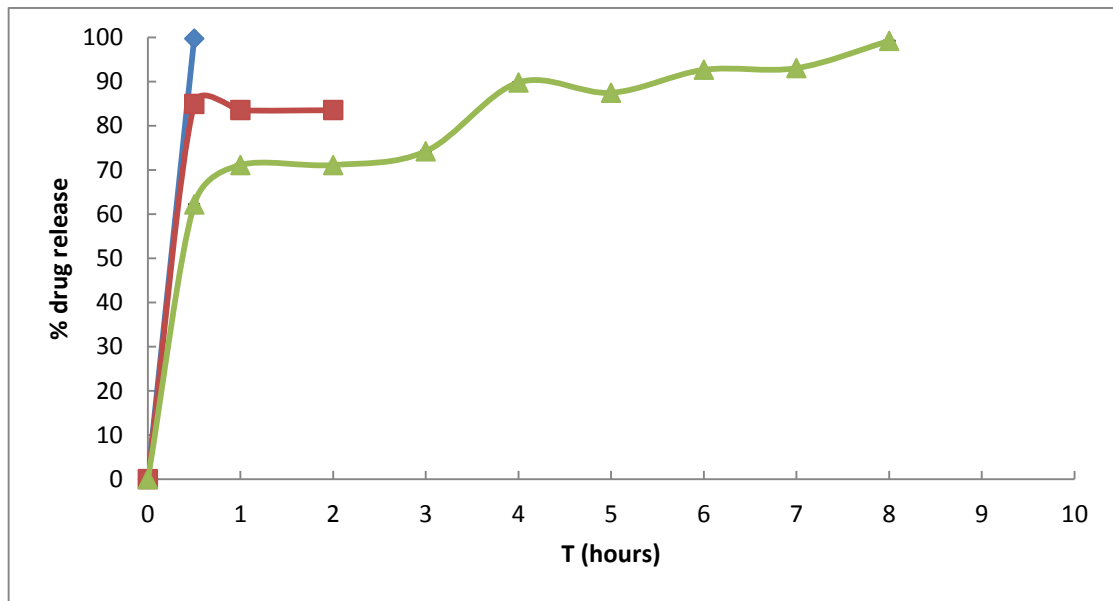


582

583 **Figure 7. a.** Circular dichroism spectra in the far-UV and **b.** infrared spectra in the
584 Amide I and II region of three representative solutions at $C_{\text{INS}} = 0.07, 0.26$ and 0.4
585 mg/ml of QNPHOSEO:INS system at $\text{pH}=7.4$ and 0.154M NaCl. The spectrum of
586 neat INS at 1 mg/ml concentration and same solution conditions is included for
587 comparison.

588

589



590

591 **Figure 8.** Cumulative INS release from three different QNPHOSEO based
592 nanocarriers (whereas the initial concentration of protein was $C_{INS}=0.027$ mg/ml –red
593 line, $C_{INS}=0.067$ mg/ml –blue line and $C_{INS}=0.260$ mg/ml –green line) 37°C in PBS.
594 Mean of three independent experiments run in triplicate, $SD<10\%$.

595

596

597 **Caption List**

598 **Figure 1. a.** Molecular structure of QNPHOSEO block polyelectrolyte (the degrees of
599 polymerization are $m=162$ and $n=334$) **b.** Schematic representation of the formation
600 of QNPHOSEO:INS complexes.

601

602 **Figure 2. (a)** Hydrodynamic radius, R_h , and **(b)** light scattering intensity at 90° , I , as
603 a function of C_{INS} , for the solutions of QNPHOSEO:INS system at $pH=7.00$ and
604 $0.01M$ NaCl (blue points) and at $pH=7.40$ and $0.154M$ NaCl (red points).

605 **Figure 3. (a)** ζ -potential and **(b)** R_g/R_h as a function of C_{INS} , for the solutions of
606 QNPHOSEO:INS system at $pH=7.00$ and $0.01M$ NaCl (blue points) and at $pH=7.40$
607 and $0.154M$ NaCl (red points).

608 **Figure 4. (a)** Hydrodynamic radius, R_h , and **(b)** ζ -potential as a function of C_{INS} , for
609 the solutions of QNPHOSEO:INS complexes as prepared at **$pH=7.4$ and $0.154M$**
610 NaCl (blue points) and after dilution in FBS:PBS 10% (v/v) (red points).

611 **Figure 5. (a)** Hydrodynamic Radius, R_h , and **(b)** ζ -potential as a function of C_{INS} , for
612 the solutions of QNPHOSEO:INS complexes as prepared at $pH=7$ and $0.01M$ NaCl
613 (blue points) and after dilution in FBS:PBS 10%(v/v) (red points).

614 **Figure 6. (a)** Hydrodynamic radius, R_h , **(b)** light scattering intensity at 90° , I , and **(c)**
615 R_g/R_h , as a function of the added NaCl concentration of representative solutions,
616 corresponding to low ($C_{INS}=0.027mg/ml$ –blue points and $C_{INS}=0.067mg/ml$ –red
617 points) and high ($C_{INS}=0.260mg/ml$ –green points) C_{INS} , of the QNPHOSEO:INS
618 complexes prepared at $pH=7.4$ and $I=0.154M$.

619 **Figure 7. a.** Circular dichroism spectra in the far-UV and **b.** infrared spectra in the
620 Amide I and II region of three representative solutions at $C_{INS}= 0.07, 0.26$ and 0.4
621 mg/ml of QNPHOSEO:INS system at $pH=7.4$ and $0.154M$ NaCl. The spectrum of
622 neat INS at $1 mg/ml$ concentration and same solution conditions is included for
623 comparison.

624 **Figure 8.** Cumulative INS release from three different QNPHOSEO based
625 nanocarriers (whereas the initial concentration of protein was $C_{INS}=0.027 mg/ml$ –red
626 line, $C_{INS}=0.067 mg/ml$ –blue line and $C_{INS}=0.260 mg/ml$ –green line) $37^\circ C$ in PBS.
627 Mean of three independent experiments run in triplicate, $SD<10\%$.

628